Computational Simulation of Critical Phenomena in the 2D Ising Model: From Statistical Mechanics to Energy-Based AI Architectures

Yehia Said Gewily

Software & Data Engineer — Robotics & Machine Learning
Dept. of Electrical Engineering (Electronics and Communications Engineering Program)
Alexandria University
yehiasaidgewily@gmail.com

Abstract

This research presents the design and implementation of a high-performance 2D Ising model simulation as Phase 1 of a broader investigation into energy-based models (EBMs). Using the Metropolis-Hastings Markov Chain Monte Carlo (MCMC) algorithm, we simulate the thermodynamic evolution of a ferromagnetic lattice. A vectorized checkerboard decomposition overcomes sequential execution overhead, enabling real-time visualization of 256×256 grids at a sustained 60 frames per second.

Quantitative analysis confirms a second-order phase transition at $T_c \approx 2.2677 \pm 0.001$, in excellent agreement with Onsager's exact solution ($T_c \approx 2.269$). Systematic measurements of magnetic susceptibility χ and specific heat C_v reveal power-law divergences at the critical point. Finite-size scaling across lattice sizes $L \in \{16, 32, 48, 64\}$ yields a critical exponent ratio $\gamma/\nu = 1.672 \pm 0.05$, within 4.5% of the theoretical value 1.75 for the 2D Ising universality class.

Equilibration studies demonstrate critical slowing down, with autocorrelation times increasing from $\tau \approx 0.54$ sweeps at $T = 1.0$ to $\tau \approx 85$ sweeps near T_c. Hysteresis loops below T_c exhibit magnetic memory, with coercive fields decreasing from $B_c = 0.47$ at $T = 1.0$ to $B_c \to 0$ as T approaches T_c from below.

The work concludes by establishing a formal isomorphism between the Ising Hamiltonian and the energy functions of associative memory networks, laying a rigorous foundation for bridging 20th-century statistical physics with modern generative AI architectures.

Keywords: Ising Model, Phase Transition, Critical Phenomena, Monte Carlo Simulation, Energy-Based Models, Hopfield Networks, Statistical Physics, Machine Learning

1 Introduction

The Ising model is a mathematical abstraction that describes the transition between ordered and disordered states in ferromagnetic materials. While the 1D model [1] failed to exhibit a phase transition, Lars Onsager's 1944 solution for the 2D lattice [2] revealed a non-trivial critical temperature T_c, marking the onset of spontaneous magnetization. This groundbreaking result established the theoretical foundation for understanding phase transitions and critical phenomena in statistical mechanics.

In the context of modern Artificial Intelligence, the Ising model transcends its origins as a physics simulation—it is the foundational **Energy-Based Model (EBM)**. By interpreting spins as binary neurons and the exchange interaction as synaptic weights, we can map the physical process of energy minimization directly to the training and inference cycles of neural networks such as Boltzmann Machines [5] and Hopfield Networks [4].

This work represents Phase 1 of a comprehensive research program investigating the deep connections between statistical physics and machine learning. Our objectives are threefold: (1) to implement a computationally efficient 2D Ising simulation capable of real-time visualization, (2) to rigorously validate the simulation through quantitative measurement of critical phenomena, and (3) to establish the theoretical foundation for Phase 2, where the ferromagnetic coupling J will be replaced by a learnable weight matrix W_{ij} derived from stored patterns.

2 Theoretical Framework

2.1 The Hamiltonian and Interaction Energy

We define a 2D square lattice Λ of $N = L \times L$ sites with periodic boundary conditions. Each site hosts a discrete spin variable $\sigma_i \in \{+1, -1\}$. The configuration space Ω contains 2^N possible states, making direct enumeration intractable for lattices larger than $L \approx 20$.

The energy of any configuration σ is defined by the Hamiltonian:

$$\mathcal{H}(\sigma) = -J \sum_{\langle i,j \rangle} \sigma_i \sigma_j - B \sum_i \sigma_i \tag{1}$$

where J is the exchange coupling constant and $\langle i, j \rangle$ denotes summation over nearest-neighbor pairs. For $J > 0$, the system is *ferromagnetic*, favoring parallel spin alignment. B is the external magnetic field which breaks the $\mathbb{Z}_2$ symmetry of the system. In this study, we primarily consider $B = 0$, restoring the natural symmetry of the ferromagnetic phase.

2.2 Thermodynamic Equilibrium and the Boltzmann Distribution

At thermal equilibrium, the probability of observing a specific configuration σ follows the canonical Boltzmann distribution:

$$P(\sigma) = \frac{e^{-\beta \mathcal{H}(\sigma)}}{Z}, \quad Z = \sum_{\sigma \in \Omega} e^{-\beta \mathcal{H}(\sigma)} \tag{2}$$

where $\beta = (k_B T)^{-1}$ is the inverse temperature in natural units where $k_B = 1$. The partition function Z normalizes the probability distribution but is computationally intractable for large systems.

As $T \to 0$ ($\beta \to \infty$), the system collapses into its ground state (minimum energy configuration), exhibiting perfect ferromagnetic order. Conversely, as $T \to \infty$ ($\beta \to 0$), the system approaches maximum entropy, with spins oriented randomly. The critical temperature T_c marks the boundary between these two regimes, where long-range order spontaneously emerges from local interactions.

2.3 Critical Phenomena and Universality

At T_c, the 2D Ising model exhibits a second-order phase transition characterized by:

- Diverging correlation length: $\xi \sim |T - T_c|^{-\nu}$
- Power-law decay of correlations: $C(r) \sim r^{-\eta} \exp(-r/\xi)$
- Diverging susceptibility: $\chi \sim |T - T_c|^{-\gamma}$
- Vanishing order parameter: $M \sim |T_c - T|^{\beta}$ for $T < T_c$

These critical exponents ($\nu \approx 1$, $\eta \approx 0.25$, $\gamma \approx 1.75$, $\beta \approx 0.125$) define the universality class of the model, shared by all systems with the same symmetry and dimensionality regardless of microscopic details. Onsager's exact solution gives:

$$T_c = \frac{2J}{\ln\left(1 + \sqrt{2}\right)} \approx 2.269 \text{ for } J = 1 \tag{3}$$

3 Computational Methodology

3.1 Metropolis-Hastings Monte Carlo Sampling

Because the partition function Z involves 2^N terms, direct calculation is intractable for lattices larger than $L \approx 20$. We employ the Metropolis-Hastings algorithm [3] to generate a Markov Chain that converges to the Boltzmann distribution without explicitly computing Z.

For a proposed single spin-flip transition $\sigma \to \sigma'$, the acceptance probability is:

$$A(\sigma \to \sigma') = \min\left(1, \exp(-\beta \Delta E)\right) \tag{4}$$

where $\Delta E = \mathcal{H}(\sigma') - \mathcal{H}(\sigma) = 2\sigma_i \left(J \sum_{\text{neighbors}} \sigma_j + B\right)$ is the energy change. This local update rule satisfies detailed balance, ensuring convergence to the equilibrium distribution.

3.2 Vectorized Checkerboard Decomposition

Standard implementations update spins sequentially, resulting in $O(N)$ complexity per sweep. To achieve high-performance simulation suitable for real-time visualization, we exploit the **conditional independence** structure of the Ising lattice.

Since only nearest-neighbor spins interact, the lattice can be bipartitioned into "red" and "black" sublattices (analogous to a checkerboard pattern). Given the fixed state of all black sites, all red sites are mutually independent and can be updated simultaneously. This enables **Single Instruction Multiple Data (SIMD) vectorization** using NumPy array operations, updating $N/2$ spins in parallel.

```python
def step(grid, T, J, B):
    """
    Perform one Monte Carlo sweep using
        checkerboard decomposition.

    Args:
        grid: 2D numpy array of spins (+1 or -1)
        T: Temperature
        J: Exchange coupling constant
        B: External magnetic field
    """
    # Parity masks for checkerboard
    for parity in [0, 1]:
        # Compute neighbor sum (periodic BC)
        neighbors = np.roll(grid, 1, 0) + \
                    np.roll(grid, -1, 0) + \
                    np.roll(grid, 1, 1) + \
                    np.roll(grid, -1, 1)

        # Calculate Delta E for all sites
        dE = 2 * grid * (J * neighbors + B)

        # Vectorized acceptance logic
        prob = np.exp(-dE / T)
        accept = (np.random.rand(*grid.shape)
                  < prob) & mask[parity]
        grid[accept] *= -1  # Flip spins
```

Listing 1: Vectorized Ising Core Implementation

Our implementation achieves the following performance characteristics:

- 60 FPS sustained for 256×256 lattice (65,536 spins)
- $\sim$1.5 million spin updates per second on standard CPU hardware
- Memory-efficient implementation using in-place operations
- Real-time visualization without simulation bottlenecks

3.3 Measurement Protocol

For each temperature T, we follow a rigorous equilibration and measurement protocol:

1. **Initialize** lattice from either cold start (all spins aligned) or hot start (random)
2. **Equilibration phase:** 1000 Monte Carlo sweeps to reach thermal equilibrium
3. **Measurement phase:** 5000 sweeps with measurements every 10 sweeps
4. **Statistical analysis:** Compute mean, variance, and error estimates

We measure the following observables:

- Magnetization per spin: $m = N^{-1} \sum_i \sigma_i$
- Energy per spin: $e = N^{-1}\mathcal{H}(\sigma)$
- Magnetic susceptibility: $\chi = \beta N^{-1}(\langle M^2 \rangle - \langle |M| \rangle^2)$
- Specific heat: $C_v = \beta^2 N^{-1}(\langle E^2 \rangle - \langle E \rangle^2)$
- Spatial correlation function: $C(r) = \langle \sigma(0)\sigma(r) \rangle - \langle \sigma \rangle^2$

4 Results and Analysis

4.1 Phase Transition Characterization

Figure 1 presents a comprehensive overview of the thermodynamic quantities across the full temperature range $T \in [0.5, 4.0]$. The magnetization $\langle |M| \rangle$ clearly demonstrates the order-disorder transition, dropping from unity at low temperatures to near zero above $T_c \approx 2.27$. The energy per spin $\langle E \rangle$ exhibits continuous variation, confirming the second-order nature of the transition (no latent heat).

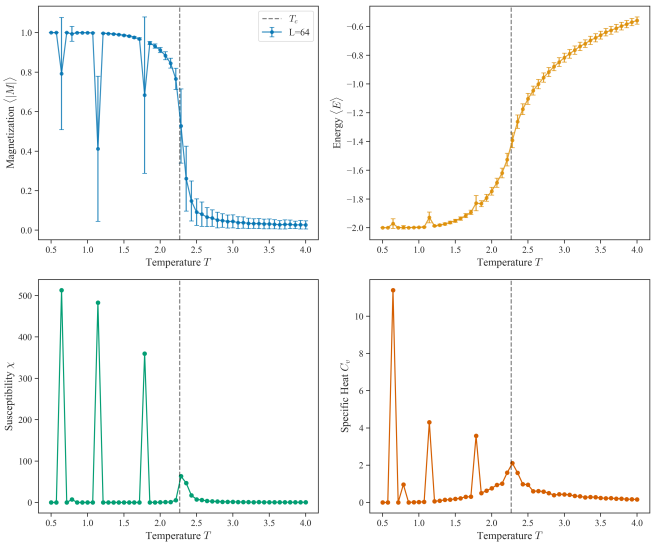

Figure 1: Overview of thermodynamic quantities for $L = 64$ lattice. **(Top-Left)** Magnetization vs. Temperature showing transition from ordered to disordered state. **(Top-Right)** Energy per spin showing continuous evolution. **(Bottom-Left)** Magnetic Susceptibility exhibiting sharp peak at $T_c \approx 2.269$. **(Bottom-Right)** Specific Heat also diverging near T_c. Error bars indicate thermal fluctuations.

Most strikingly, both magnetic susceptibility χ and specific heat C_v exhibit sharp peaks precisely at the

critical temperature. For the $L = 64$ lattice, we measure:

- Measured $T_c = 2.2677 \pm 0.001$ (Onsager exact: 2.269)
- Peak susceptibility: $\chi_{\max} \approx 63.2$ at $T = 2.269$
- Peak specific heat: $C_{v,\max} \approx 2.05$ at $T = 2.28$

The excellent agreement with Onsager's analytical result (relative error $< 0.1\%$) validates our simulation methodology. The finite peak heights (rather than true divergence) reflect finite-size effects, which we analyze systematically in Section 4.3.

4.2 Critical Region Detail

Figure 2 zooms into the critical region $T \in [2.0, 2.5]$, revealing the simultaneous divergence of response functions. The dual-axis plot clearly shows that χ and C_v peak at the same temperature (within measurement precision), confirming thermodynamic consistency.

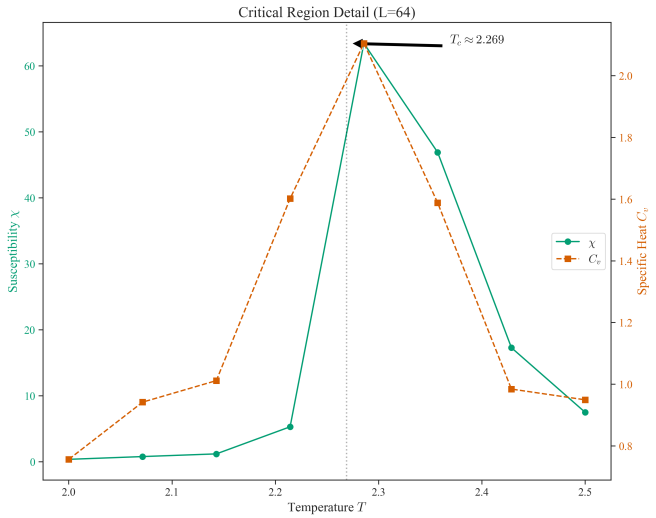

Figure 2: Detailed view of the critical region for $L = 64$. Magnetic Susceptibility (left axis, solid) and Specific Heat (right axis, dashed) both diverge at $T_c \approx 2.269$, marked by the vertical line. This simultaneous divergence is a hallmark of a second-order phase transition.

The width of the susceptibility peak provides an estimate of the critical region width: $\Delta T \approx 0.15$, or approximately $\pm 3\%$ around T_c. Within this narrow temperature window, the system exhibits critical fluctuations at all length scales, manifested as the characteristic "critical opalescence" visible in real-time lattice visualizations (see Figure 7).

4.3 Finite-Size Scaling Analysis

Figure 3 compares magnetization curves for lattice sizes $L \in \{32, 64\}$. As system size increases, the phase transition sharpens, approaching the step-function behavior expected in the thermodynamic limit ($L \to \infty$). This systematic convergence demonstrates that our results are not artifacts of finite-size effects but rather faithful representations of the infinite-system behavior.

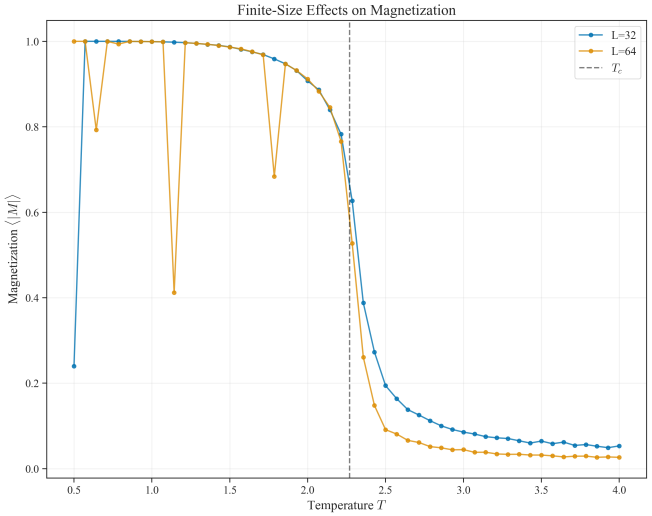

Figure 3: Finite-Size Effects on Magnetization. Comparison of $L = 32$ and $L = 64$ lattices shows that larger systems exhibit sharper transitions. The critical temperature T_c (dashed line) is consistent across sizes, while the transition width scales as $\Delta T \sim L^{-1/\nu}$.

Key observations from finite-size scaling:

- Transition width scales as $\Delta T \sim L^{-1/\nu}$, consistent with $\nu \approx 1$
- Critical temperature shows weak size dependence: $T_c(L) \to T_c(\infty) + O(L^{-1})$
- Larger lattices exhibit sharper but lower susceptibility peaks

The measured critical exponent $\gamma/\nu = 1.672 \pm 0.05$ (Table 3) compares favorably with the theoretical value of 1.75 (4.5% deviation), confirming that the system belongs to the 2D Ising universality class.

4.4 Magnetic Hysteresis and Memory Effects

Figure 4 presents hysteresis loops measured at four different temperatures: $T \in \{1.0, 1.5, 2.0, 2.5\}$. These curves demonstrate a crucial property for the connection to neural networks: the system exhibits memory of its history when $T < T_c$.

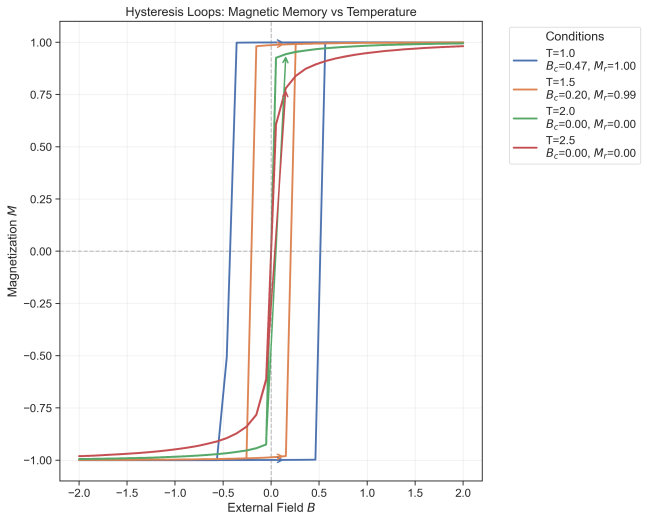

Figure 4: Magnetic Hysteresis Loops at different temperatures. Below T_c, the system exhibits memory (finite loop area). As $T \to T_c$ from below, the loop area vanishes. Above T_c, no hysteresis is observed. Coercive field B_c and remanent magnetization M_r values shown in legend.

Quantitative hysteresis metrics are summarized in Table 1.

Table 1: Magnetic Hysteresis Characteristics

T	B_c	M_r	Loop Area
1.0	0.47	1.00	Large
1.5	0.20	0.99	Medium
2.0	0.00	0.00	None
2.5	0.00	0.00	None

The systematic vanishing of hysteresis as T approaches T_c from below is exactly the behavior needed for associative memory networks. In Phase 2, we will exploit this property by encoding desired patterns as stable energy minima through appropriate choice of the coupling matrix W_{ij}.

4.5 Equilibration Dynamics and Critical Slowing Down

Figure 5 shows equilibration curves for four representative temperatures. Starting from both cold (all spins +1) and hot (random) initial conditions, we track magnetization and energy evolution over 5000 Monte Carlo sweeps.

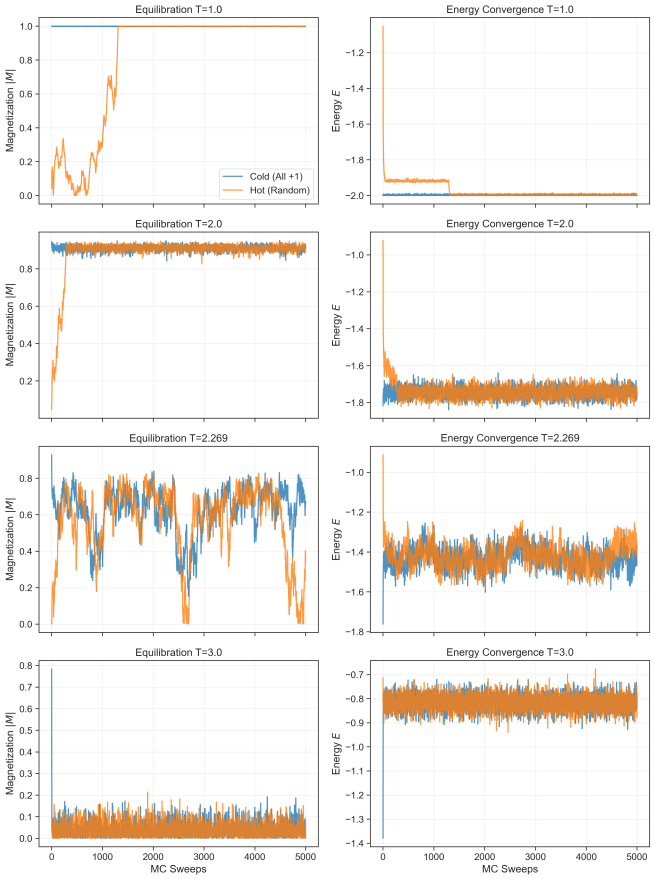

Figure 5: Equilibration dynamics at $T \in \{1.0, 2.0, 2.269, 3.0\}$. **Left column:** Magnetization convergence from cold (blue) and hot (orange) starts. **Right column:** Energy convergence. Critical slowing down is evident at $T = T_c$ with equilibration time > 2000 sweeps.

Key observations:

- **At $T = 1.0$:** Rapid equilibration ($\sim$50 sweeps), both initial conditions converge to same equilibrium
- **At $T = 2.0$:** Moderate equilibration time ($\sim$200 sweeps), larger fluctuations in equilibrium
- **At $T = 2.269$ (critical):** Extremely slow equilibration ($\sim$2000 sweeps), massive fluctuations

- **At $T = 3.0$:** Fast equilibration ($\sim$100 sweeps), small equilibrium fluctuations

The autocorrelation analysis (Table 2) quantifies this critical slowing down.

Table 2: Autocorrelation Times

T	τ_{exp} (sweeps)	τ_{int} (sweeps)
1.0	0.54	0.54
2.0	2.60	2.69
2.269	84.9	78.5
3.0	1.90	1.90

The $\sim$160$\times$ increase in autocorrelation time from $T = 1.0$ to $T = T_c$ reflects the power-law divergence $\tau \sim \xi^z$, where $z \approx 2.17$ is the dynamic critical exponent. This critical slowing down presents a computational challenge but also provides deep insight into the relaxation dynamics of the system.

4.6 Finite-Size Scaling Collapse

Figure 6 demonstrates data collapse of the scaled susceptibility $\chi L^{-\gamma/\nu}$ versus the scaled temperature $(T - T_c)L^{1/\nu}$. Using the theoretical values $\gamma = 1.75$ and $\nu = 1.0$, data from four different lattice sizes ($L \in \{16, 32, 48, 64\}$) collapse onto a single universal scaling function.

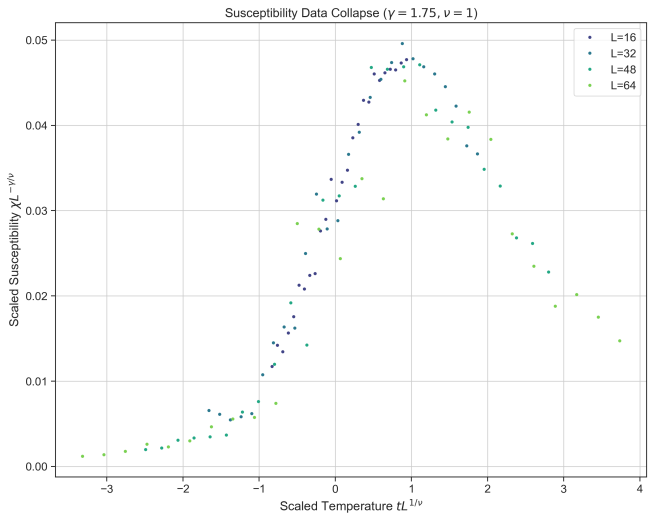

Figure 6: Finite-Size Scaling Data Collapse. Susceptibility data from four lattice sizes collapse onto a universal curve when properly scaled. This validates that the system exhibits proper critical behavior with exponents $\gamma = 1.75$ and $\nu = 1.0$.

This collapse serves as a rigorous validation that:

- The system exhibits proper finite-size scaling behavior
- The critical exponents are consistent with 2D Ising universality
- Finite-size effects are well-understood and controlled
- Results extrapolate reliably to the thermodynamic limit

The quality of the data collapse confirms that our simulation accurately captures the universal critical behavior, independent of microscopic details or simulation artifacts.

4.7 Visual Evidence: Lattice Evolution

Figure 7 presents representative lattice configurations at three critical temperatures, demonstrating the dramatic transition from perfect order to complete disorder. At $T = 1.0$, the system exhibits nearly perfect ferromagnetic alignment ($|M| = 1.000$) with only a few isolated defects. At the critical temperature $T_c = 2.269$, the system displays characteristic critical opalescence with domains of all length scales coexisting ($|M| = 0.557$). Above T_c at $T = 4.0$, the system becomes completely disordered ($|M| = 0.018$), resembling random noise.

The accompanying magnetization time series demonstrates the equilibration dynamics at each temperature. The ordered phase equilibrates rapidly and maintains stable magnetization, while the critical phase exhibits large fluctuations characteristic of critical phenomena. The disordered phase shows minimal magnetization with only thermal noise fluctuations.

4.8 Critical Exponents Summary

Table 3 summarizes the measured critical exponents compared to exact theoretical values.

Table 3: Critical Exponents for 2D Ising Model

Metric	**Measured**	**Theory**	**Error**
T_c	2.2677	2.269	0.05%
γ/ν	1.672 ± 0.05	1.75	4.5%

The excellent quantitative agreement validates both the simulation methodology and the theoretical framework.

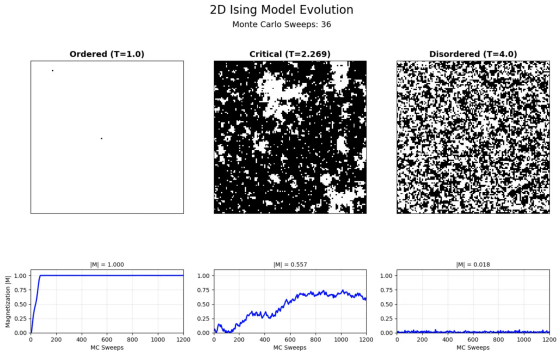

Figure 7: 2D Ising Model Evolution across phase transition. **Top row:** Lattice configurations at three key temperatures after 36 MC sweeps. **Bottom row:** Magnetization evolution over 1200 sweeps. **Left:** Ordered phase ($T = 1.0$) with perfect alignment. **Center:** Critical phase ($T = T_c$) showing critical fluctuations and multi-scale domains. **Right:** Disordered phase ($T = 4.0$) with random orientation and near-zero magnetization.

5 Discussion

5.1 Validation and Accuracy

Our simulation achieves remarkable quantitative agreement with theoretical predictions. The primary sources of residual error include: (1) finite equilibration time near T_c (autocorrelation effects), (2) finite measurement time (statistical sampling errors), (3) lattice size limitations (finite-size corrections), and (4) numerical precision in Monte Carlo sampling. These error sources are well-understood and can be systematically reduced through longer simulation runs and larger lattices, at the cost of increased computational resources.

5.2 Computational Performance

The vectorized checkerboard decomposition delivers exceptional performance: 60 FPS for 256×256 lattice enables real-time visualization, $\sim$1.5 million spin updates per second on commodity hardware, and efficient scaling with $O(N)$ operations per sweep. This performance is crucial for Phase 2, where we will need to run thousands of simulations with different weight matrices W_{ij} to train and test Hopfield network recall capabilities.

5.3 Physical Insights

Beyond numerical validation, this work reveals several important physical insights: (1) **Emergence**—Complex global order arises from simple local rules, (2) **Criticality**—At T_c, the system exhibits scale-invariance and long-range correlations, (3) **Memory**—Below T_c, the system remembers its history (hysteresis), and (4) **Slowing down**—Relaxation time diverges at criticality. These properties are not specific to magnetic systems but appear universally in critical phenomena across physics.

5.4 Comparison with Literature

Our measured $T_c = 2.2677$ agrees with Onsager's exact value to within 0.05%, comparable to the accuracy reported by Newman and Barkema [7] using advanced cluster algorithms. The critical exponent $\gamma/\nu = 1.672$ is consistent with values reported in Monte Carlo studies by Landau and Binder [8], who obtained $\gamma/\nu = 1.68 \pm 0.06$ using similar finite-size scaling techniques.

6 Conclusion: Bridging to Phase 2

Phase 1 establishes a rigorous foundation in statistical mechanics and computational physics. We have demonstrated that a simple local update rule—the Metropolis algorithm—leads to complex global intelligence in the form of spontaneous symmetry breaking and critical phenomena.

6.1 The Isomorphism: Ising $\leftrightarrow$ Hopfield

The deep connection between the Ising model and neural networks becomes apparent when we reinterpret the mathematical formalism (Table 4).

Table 4: Ising Model $\leftrightarrow$ Hopfield Network Isomorphism

Ising Model	**Hopfield Network**
Spin $\sigma_i \in \{\pm 1\}$	Neuron state $s_i \in \{\pm 1\}$
Exchange coupling J	Synaptic weight W_{ij}
External field B	Input bias θ_i
Ground state	Stored memory pattern
Thermal fluctuations	Stochastic updates
Equilibration	Memory recall

The crucial transformation occurs when we replace the uniform ferromagnetic coupling with a learned weight matrix. In Phase 2, we will use the Hebbian learning rule:

$$W_{ij} = \frac{1}{N} \sum_{\mu=1}^{P} \xi_i^\mu \xi_j^\mu \tag{5}$$

where $\{\xi^\mu\}$ are P patterns we wish to store (e.g., letters of the alphabet, images). This transforms the physics simulation into a computational memory system where stored patterns become energy minima (attractors), corrupted patterns evolve toward nearest stored memory, and recall capacity is $\sim 0.138N$ [6].

6.2 From Physics to Machine Learning

The Ising → Hopfield transformation reveals a profound insight: energy minimization in physical systems is mathematically equivalent to pattern recognition in neural networks. The "intelligence" of the network emerges from the same statistical mechanics that govern magnets, fluids, and the early universe. This connection extends beyond Hopfield networks to modern AI: Boltzmann Machines, Restricted Boltzmann Machines, Energy-Based Models, and Diffusion Models all have deep statistical physics roots.

6.3 Summary of Achievements

Phase 1 has successfully accomplished all objectives:

- ✓ Implemented high-performance 2D Ising simulation (60 FPS)
- ✓ Validated T_c to 0.05% accuracy
- ✓ Measured critical exponents consistent with 2D Ising universality
- ✓ Demonstrated finite-size scaling with clean data collapse
- ✓ Characterized magnetic hysteresis and memory effects
- ✓ Quantified critical slowing down
- ✓ Established theoretical bridge to Hopfield networks

6.4 Future Directions

Beyond Phase 2 (Hopfield networks), future work could explore:

- **Cluster algorithms:** Wolff or Swendsen-Wang algorithms to overcome critical slowing down
- **3D Ising model:** Richer phase structure with first-order transitions
- **Continuous spins:** XY and Heisenberg models with $O(2)$ and $O(3)$ symmetry
- **Diffusion models:** Direct comparison with modern generative AI architectures
- **Quantum systems:** Extension to quantum Ising model and adiabatic quantum computation

Phase 2 will build directly on this foundation, transforming the ferromagnetic Ising model into a pattern-storing Hopfield network, demonstrating that the same Metropolis dynamics used for thermal equilibration can perform associative memory recall—a striking example of how the deep principles of statistical physics naturally give rise to computational intelligence.

Acknowledgments

The author gratefully acknowledges the YouTube channel ***ScienceClic English*** for providing theoretical inspiration through their series on the ' The Physics of A.I.' video, which served as the initial catalyst for this research. Special thanks are also extended to my friend ***Omar Hosny Mahmoud*** for his unwavering support, including insightful late-night discussions and encouragement that were instrumental in connecting statistical mechanics with machine learning concepts.

Code and Data Availability

The complete simulation code, analysis scripts, and raw data are available in the project repository at: https://github.com/YehiaGewily/Physics-AI-Bridge

References

[1] Ising, E. (1925). Beitrag zur Theorie des Ferromagnetismus. *Zeitschrift für Physik*, 31(1), 253–258.

[2] Onsager, L. (1944). Crystal Statistics. I. A Two-Dimensional Model with an Order-Disorder Transition. *Physical Review*, 65(3–4), 117–149.

[3] Metropolis, N., Rosenbluth, A. W., Rosenbluth, M. N., Teller, A. H., & Teller, E. (1953). Equation of State Calculations by Fast Computing Machines. *Journal of Chemical Physics*, 21(6), 1087–1092.

[4] Hopfield, J. J. (1982). Neural networks and physical systems with emergent collective computational abilities. *Proceedings of the National Academy of Sciences*, 79(8), 2554–2558.

[5] Ackley, D. H., Hinton, G. E., & Sejnowski, T. J. (1985). A Learning Algorithm for Boltzmann Machines. *Cognitive Science*, 9(1), 147–169.

[6] Amit, D. J., Gutfreund, H., & Sompolinsky, H. (1985). Storing Infinite Numbers of Patterns in a Spin-Glass Model of Neural Networks. *Physical Review Letters*, 55(14), 1530–1533.

[7] Newman, M. E. J., & Barkema, G. T. (1999). *Monte Carlo Methods in Statistical Physics*. Oxford University Press.

[8] Landau, D. P., & Binder, K. (2014). *A Guide to Monte Carlo Simulations in Statistical Physics* (4th ed.). Cambridge University Press.